Soft Matter

Growth of Au and ZnS nanostructures via engineered peptide and M13 bacteriophage templates

Journal:	*Soft Matter*
Manuscript ID	SM-COM-01-2018-000090.R1
Article Type:	Communication
Date Submitted by the Author:	23-Mar-2018

Complete List of Authors:	Chung, Sungwook; Pusan National University, School of Chemical and Biomolecular Engineering; E O Lawrence Berkeley National Laboratory, The Molecular Foundry; E O Lawrence Berkeley National Laboratory, Physical Biosciences Division Chung, Woo-Jae; Sungkyunkwan University, Department of Integrative Biotechnology, College of Biotechnology and Bioengineering; E O Lawrence Berkeley National Laboratory, The Molecular Foundry; E O Lawrence Berkeley National Laboratory, Materials Sciences Division Wang, Debin; E O Lawrence Berkeley National Laboratory, The Molecular Foundry; E O Lawrence Berkeley National Laboratory, Materials Sciences Division; Pacific Northwest National Laboratory, Physical Sciences Division Lee, Seung-Wuk; University of California, Department of Bioengineering; E O Lawrence Berkeley National Laboratory, Materials Sciences Division De Yoreo, James; Pacific Northwest National Laboratory, Physical Sciences Division; E O Lawrence Berkeley National Laboratory, The Molecular Foundry; E O Lawrence Berkeley National Laboratory, Materials Sciences Division; University of Washington, Department of Materials Science and Engineering

Soft Matter

COMMUNICATION

Growth of Au and ZnS nanostructures via engineered peptide and M13 bacteriophage templates

Received 00th January 20xx,
Accepted 00th January 20xx

DOI: 10.1039/x0xx00000x

www.rsc.org/

Sungwook Chung,[a,c,e] Woo-Jae Chung,[a,b,f] Debin Wang,[a,b,g] Seung-Wuk Lee [b,d*] and James J. De Yoreo[a,b,g,h*]

We demonstrate directed nucleation of Au and ZnS patterns on templates comprised of functional peptides and M13 bacteriophage. We discuss the control over nucleation in terms of the interplay between enhanced ion binding and reduced interfacial energy resulting from the presence of the templates.

Introduction

In vitro biopanning approaches for selecting biomolecules have been successful in discovering peptides and oligonucleotides with high binding affinity to proteins and catalytic activities towards chemical reactions.[1] These methods have also been tailored to the discovery of biomolecules with high binding affinities to inorganic nanomaterials.[2-4] Early studies demonstrated a correlation between biomolecules possessing high binding affinity to inorganic materials and their ability to mediate the formation of those materials.[5] For example, peptides with high binding affinities toward inorganic materials were shown to be involved in the reduction or clustering of inorganic ions into solids during mineralization.[6] More recently, a mechanistic basis for this correlation was demonstrated through theory and experiment, which showed that binding affinity of bioorganic templates for crystal surfaces is inherently related to the interfacial energy that determines the free energy barrier to nucleation on those templates.[7] However, many aspects of this process have yet to be explored, including the kinetic controls, the effect of additives, and the relationship between template dimension, nucleation density and the uniformity of the resulting crystalline films. Understanding the role of peptides during the mineralization processes is of fundamental importance because it has the potential to enable creation of inorganic nanomaterials with well-defined size, shape, and composition exhibiting a degree of fidelity typically achieved by living organisms during biomineralization processes.[8-11]

Here, we present work aimed at developing a generic platform of biochemical templates and testing their ability to create spatially well-defined patterns of inorganic materials on surfaces. We first developed methods of fabricating templates of immobilized functional peptides and M13 bacteriophage via two-step μ-contact soft lithography. These templates were used to mediate the subsequent formation of Au and ZnS nanostructures on the surfaces of the templates. Our results show that templates patterned with a gold binding peptide (GBP) induce the formation of Au nanoparticles and that the coverage and particle size distribution can be dramatically improved by the addition of silver (Ag^+) ions to the precursor solutions. Templates patterned with three different zinc sulfide (ZnS) binding peptides (ZBPs) induced the formation of ZnS nanostructures, however the coverage of ZnS was relatively low when compared to the Au films on GBPs. In contrast, when M13 bacteriophage was genetically engineered to express EEEE tetra-glutamate residues, a major portion of the two ZBP sequences selected through biopanning, in its surface coat protein *p8*, templates patterned with the engineered M13 bacteriophage induced the formation of ZnS films 10's of nanometer in thickness and exhibiting high coverage.

Results and Discussion

[a] *The Molecular Foundry, Lawrence Berkeley National Laboratory, 1 Cyclotron Road, Berkeley, California 94720, USA.*
[b] *Materials Sciences Division, Lawrence Berkeley National Laboratory, 1 Cyclotron Road, Berkeley, California 94720, USA.*
[c] *Physical Biosciences Division, Lawrence Berkeley National Laboratory, 1 Cyclotron Road, Berkeley, California 94720, USA.*
[d] *Department of Bioengineering, University of California, Berkeley, Berkeley, California 94720, USA.*
[e] *School of Chemical and Biomolecular Engineering, Pusan National University, 2, Busandaehak-ro 63Beon-gil, Geumjeong-gu, Busan 46241, South Korea.*
[f] *Department of Integrative Biotechnology, College of Biotechnology and Bioengineering, Sungkyunkwan University, Suwon 16419, South Korea.*
[g] *Physical Sciences Division, Pacific Northwest National Laboratory, Richland, Washington 99352, USA.*
[h] *Department of Materials Science and Engineering, University of Washington, Seattle, WA 98185, USA.*

†Electronic Supplementary Information (ESI) available: AFM, XPS, and TEM data of Au nanoparticles formed on templates consisting of GBP; AFM, FESEM, EDS, and current-voltage (I-V) data of ZnS nanostructures on templates of ZBP. See DOI: 10.1039/x0xx00000x

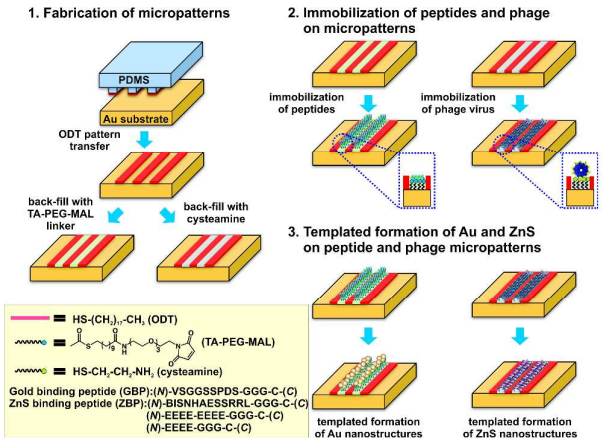

Figure 1. Schematic illustration of fabricating patterned templates of peptides and M13 bacteriophage for inducing formation of Au and ZnS nanostructures. Two-step μ-contact soft lithography was used to fabricate alternating stripes of ODT SAMs on Au surfaces and was followed by back-filling of the trenches with functional molecules such as TA-PEG-Mal and cysteamine. TA-PEG-Mal was used to attach both GBPs and ZBPs to the patterns, while cysteamine was used to assemble M13 bacteriophage on the patterns.

Figure 1 illustrates the strategy for immobilizing peptides and M13 bacteriophage on Au surfaces. We first used μ-contact soft lithography to pattern resist molecules such as 1-octadecanethiol (ODT) on Au surfaces to form a self-assembled monolayer (SAM) and then backfilled the unpatterned areas with two different types of bifunctional molecules: either TA-PEG-Mal or cysteamine. The thioacetate (TA) group of the TA-PEG-Mal is known to spontaneously decompose into a free thiol group (-SH) that can covalently bind to bare Au to form a Au-S bond *in situ* in the solution environment. Cysteamine has a free thiol group that can form the same Au-S bond. These linear patterns TA-PEG-Mal and cysteamine thus provided us with chemoselective attachment sites for either peptides such as GBP and ZBP via a cysteine (Cys) residue placed at the *C*-terminus,[12, 13] or M13 bacteriophage with terminal multiple glutamate residues such as the EEEE sequence expressed in the *pVIII* major coat protein of the M13 phage, respectively.

We used atomic force microscopy (AFM) to characterize the formation of the patterned substrates. In particular, we used lateral force microscopy (LFM), because it allows one to measure relative differences in surface frictional characteristics,[14] which can be used to investigate the degree of surface immobilization during the patterning process. Figure 2 shows AFM micrographs of the patterned substrates fabricated via μ-contact soft lithography. The resulting patterns of TA-PEG-Mal or cysteamine consisted of lines with widths of 2–4 μm separated by 4–8 μm. Figure 2 shows that AFM topographic height (Fig. 2B) and phase (Fig. 2C) micrographs of the TA-PEG-Mal linker patterns did not distinguish the alternating stripes as clearly as did the LFM micrographs (Fig. 2A).

Figure 2D shows three different profiles of the friction force measured from the linear patterns at each patterning step shown in Fig. 1 and 2. The solid black line in Fig. 2D represents the relative difference in friction force measured at the interface between the bare Au and ODT SAM resist. As the bare Au (a solid black line) was back-filled with the TA-PEG-Mal, the relative difference in friction force (solid red line) increased by about eight times. This increase was likely due to the larger friction force difference between the less hydrophobic TA-PEG-Mal SAM in the trench and the more hydrophobic ODT SAM as compared to the friction force difference between the bare Au and ODT SAM.

Once the formation of the maleimide-terminated linear patterns of TA-PEG-Mal SAM were verified by LFM, Cys-terminated peptides such as GBP and ZBP were reacted with the maleimide terminal group of the lines. The corresponding LFM profile of GBP immobilized TA-PEG-Mal SAM (a solid blue line) in Fig. 2 shows that the relative difference in friction force was slightly greater with the GBP than without it (solid red line). The increases in the relative difference of friction force measured from the linear patterns were likely due to a significant hydrophilic nature of the immobilized GBPs on TA-PEG-Mal SAM adjacent to the hydrophobic ODT SAM. Therefore, these results suggest that LFM is likely to be a valuable technique for qualitatively assessing the degree of chemoselective functionalization of the surfaces during such patterning processes.

We used the GBP immobilized patterns as templates to see if they mediated the formation of Au nanostructures. AFM height micrographs of Fig. 3 show the formation of Au nanoparticles on the alternating stripes of the GBP patterned templates. We found that the density and height of the Au nanoparticles formed on the GBP patterned templates were strongly affected by the presence of Ag^+ ions in the growth solution of aqueous auric acid (see Experimental Section). The average height of the Au nanoparticles measured from the AFM height image was found to be 21.8±3.8 nm without the Ag^+ ions (Fig. 3A1) and 6.0±0.9 nm with the Ag^+ ions (Fig. 3B1) present in the growth solution. The results also show that the presence of Ag^+ ions resulted in a far narrower size distribution (Fig. 3B1) of Au nanoparticles than was achieved without Ag^+ ions (Fig. 3A1). Furthermore, the addition of Ag^+ ions to the growth solution greatly increased the number density of Au nuclei, leading to a nearly continuous layer of Au nanoparticles with a coverage of ~93% (Fig. 3B1) as compared to ~74% (Fig. 3A1) in the absence of Ag^+ ions. Finally, as the amount of Ag^+ ions in the growth solution was increased from 1 to 30 wt. %, the average thickness of the resulting Au film formed on the patterns increased from ~5 to ~20 nm (see Fig. S1 in ESI†). Although the role of Ag^+ ions could not be fully understood, this observation suggests the idea that Ag^+ ions may act as sacrificial seeds[15] for facilitating reduction of $AuCl_4^-$ ions and forming complex ions with Cl^- from $HAuCl_4$ and therefore increasing their nucleation rate before the subsequent growth of the Au nanoparticles.

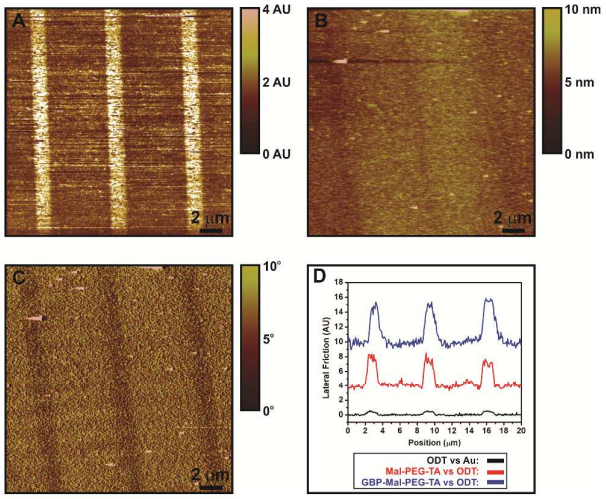

Figure 2. AFM lateral friction (A), height (B), and phase (C) images of alternating stripes of TA-PEG-Mal and ODT SAM patterns fabricated via two-step μ-contact soft lithography on Au surfaces. (D) LFM profiles across the patterns of alternating stripes show the relative difference in friction force at the interface between ODT SAM and bare Au (black), TA-PEG-Mal SAM (red), and GBP immobilized TA-PEG-Mal (blue). The profiles were shifted along the y-axis (lateral friction) for clarity.

We performed several control experiments to verify that it is indeed GBP that is involved in templating the formation of Au nanoparticles. First of all, almost no Au nanoparticles were formed on the templates patterned with TA-PEG-Mal, but lacking the GBP. Second, we verified that there were almost no Au nanoparticles formed in growth solutions with an auric acid concentrations (~1 mM) typical of those used to induce the formation of Au nanoparticles on the GBP patterned templates. Therefore, Au nanoparticles found on the GBP patterned templates did not form in the growth solution and then deposit on the templates. Finally, we confirmed via XPS and TEM that Au nanoparticles formed on the GBP patterned templates were indeed made of elemental Au (see Fig. S2 and S3 in ESI†).

The sequence of GBP was originally discovered through phage display technology for its ability to bind to Au surfaces.[16] The observation that Au nanoparticles nucleate only on the GBP patterned templates is thus consistent with the relationship between binding affinity and interfacial energy discussed above, which leads to a lowering of the free energy barrier to nucleation. However, there can also be kinetic reasons for enhanced nucleation, particularly enhanced ion binding, which can increase the local supersaturation or simply increase the kinetic pre-factor for ion attachment to a developing Au nucleus.[17] Lowering of the free energy barrier relies on the collective outcome of an ensemble of peptides binding to a nascent crystal surface[18] and thus can be expected to be highly dependent on either the organization of the peptides or their specific sequence or both. There are clear examples where the organization of an organic template is

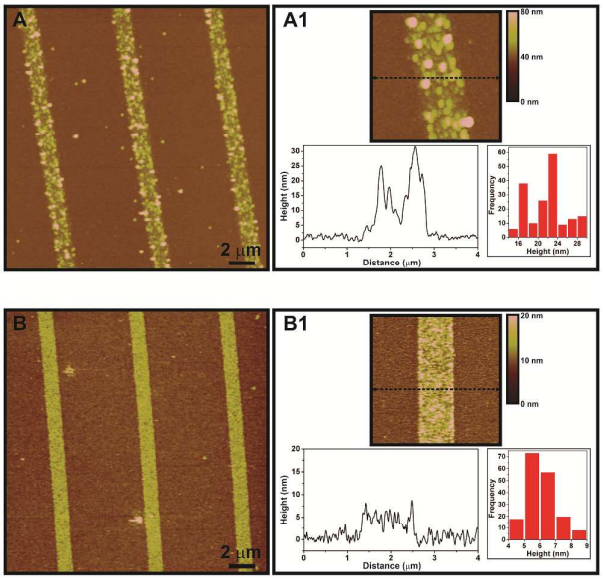

Figure 3. AFM height images of Au nanoparticles formed on templates consisting of alternating GBP stripes separated by ODT. (A) AFM height image of Au nanoparticles formed only on GBP stripes. (A1) magnified AFM height image of (A) and its height profile showing a nearly bimodal size distribution of Au nanoparticles (mean height of 21.8±3.8 nm, based on 176 counts). (B) AFM height image of Au nanoparticles formed on the same GBP patterns in the presence of Ag^+ ions in the growth solution. (B1) magnified AFM height image of (B) and its height profile showing a narrower size distribution of Au nanoparticles (mean height of 6.0±0.9 nm, based on 176 counts)

responsible for directing nucleation via this mechanism[7, 19, 20] and others[21-23] where this mechanism is inferred from theoretical predictions[24, 25] or by comparison to those for which it has been demonstrated quantitatively.[7, 19, 20] In contrast, the second mechanism is controlled by activation barriers for individual atomistic processes and thus could well depend on only one or two exposed functional groups acting independently.[18]

We tested whether the sequence of patterned GBP on the templates, particularly ones that are directly exposed towards the growth solution, play an important role in the chemical interactions responsible for enhanced nucleation of Au nanoparticles. The GBP was immobilized through a Cys (C) group at the *C*-terminus, which reacted to the maleimide group of the TA-PEG-Mal (Fig. 1). Among the residues of the GBP patterned templates, valine (V), serine (S), and glycine (G) were the three key residues positioned close to the *N*-terminus of the GBP and therefore almost completely exposed to the growth solution. Based on our hypothesis, we assumed that these three residues were involved in directing the formation of Au nanoparticles. However, when GBP was synthesized by a reverse coupling reaction that builds the peptide sequence up from the surface of the resin in an *N* to *C* rather than *C* to *N* manner and then immobilized via the Cys (C) group at the *N*-terminus rather than at the *C*-terminus,

there were almost no Au nanoparticles formed on the GBP patterned templates. Moreover, if the *N*-terminus serine (S) residue was replaced by alanine (A) or glycine (G), the coverage of Au nanoparticles formed on the GBP patterned templates was significantly reduced to ~10% or less of the number formed with the original sequence.

These results suggest that the hydroxyl side chain of the serine (S) residue is involved in the formation of Au nanoparticles. Munro et al. reported that the *N*-terminal tryptophan residue of the peptide *N*-terminus-WAGAKRLVLRRE-*C*-terminus is responsible for reducing $AuCl_4^-$ ions during the peptide mediated Au nanoparticle formation.[26] The hydroxyl side chain of the serine (S) residue may be similarly involved in reducing $AuCl_4^-$ ions. Furthermore, a potentially protonated, positively charged amino group at the *N*-terminus of the GBP combined with the hydroxyl group of the serine (S) residue could be responsible for attracting ionic Au precursors containing Au^{3+} ions electrostatically and then promoting nucleation by locally reducing the precursors.[27] These observations suggest that kinetic enhancement through ion binding is a more likely scenario for the observed templated Au nucleation reaction, though a role for reduced interfacial energy cannot be ruled out.

We applied a similar strategy to immobilize ZBPs with three different sequences (see Fig. 1) on patterned templates through the same Cys (C) group of the ZBPs at the *C*-terminus. The ZBP of *N*-terminus-BISNHAESSRRL-GGG-C-*C*-terminus was originally discovered by a phage display biopanning process.[28] However, the other two ZBPs with multiple glutamate residues were not discovered nor designed by the same process. Therefore, we used ZBP immobilized patterns as templates to see if they mediate the formation of ZnS nanostructures. One of the rationales of using multiple glutamate residues as a potential sequence for templated formation of ZnS nanostructures is that multiple glutamate residues would provide an electrostatically favourable environment for nucleation sites of ZnS, as reported elsewhere.[29]

We confirmed the formation of ZnS nanoparticles on the alternating stripes of ZBP patterned templates. However, the coverage was low as compared to that of the Au nanoparticles formed on the GBP patterned templates (see Fig. S4 in ESI†). Out of three potential ZBP sequences, two ZBPs with multiple glutamate residues (*N*-terminus-EEEE-GGG-C-*C*-terminus and *N*-terminus-EEEEEEEE-GGG-C-*C*-terminus) showed a slightly higher coverage (~20%) than that observed on average (<~5%) for *N*-terminus-BISNHAESSRRL-GGG-C-*C*-terminus.

Because the μ-contact printed patterns of ZBP failed to provide high fidelity templates, we investigated the possibility that the organization of the peptides was an important factor by employing whole M13 bacteriophage rather than ZBP as a platform to induce the formation of ZnS nanostructures. This particular phage was purposely designed so that its exposed portion of *pVIII* major coat protein had four glutamate (EEEE) residues almost identical to the multiple glutamate residues of two ZBPs shown in Fig. 1. It was previously demonstrated that this EEEE-modified phage can successfully assemble on micropatterns of cysteamine functionalized surfaces due to a strong electrostatic attractive interaction between the anionic carboxylic groups of the glutamate residues and the cationic amino groups.[30] Therefore, we used alternating stripes of cysteamine and ODT SAM on Au surfaces to assemble the EEEE expressed phage to induce the formation of ZnS nanostructures.

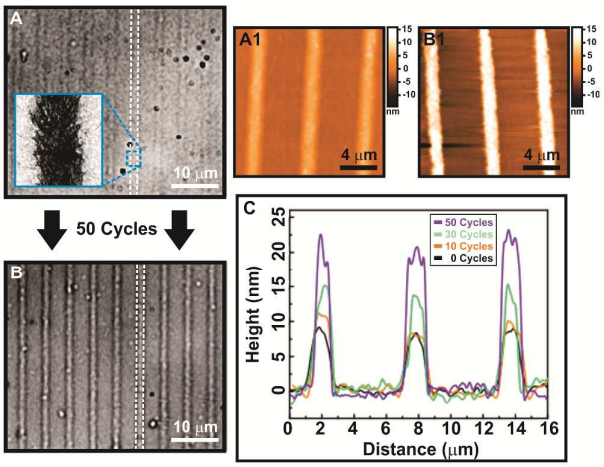

Figure 4. Optical microscopy (A) and magnified AFM height (A1) images of EEEE terminated M13 phage assembled on alternating stripes of cysteamine and ODT. Optical microscopy (B) and magnified AFM height (B1) images of the same patterns showing the formation of ZnS after 50 cycles of dipping in an aqueous solution of Zn^{2+} ions followed by a solution of S^{2-} ions. (C) AFM height profiles across the patterns of alternating stripes show the measured height of ZnS formed on EEEE terminated M13 phage depends on the number of dipping cycles. The average height of ZnS nanostructures increased to ~10 nm after 50 cycles of dipping.

Figure 4 shows optical and AFM micrographs of the EEEE expressed phage assembled on the cysteamine patterned templates before and after the formation of ZnS. The height of the phage-coated lines was measured to be ~7.2 ± 1 nm, which is almost equal to the diameter of a single M13 bacteriophage (theoretical diameter is ~6.6 nm).[31] Once the EEEE-modified phage were successfully assembled on the cysteamine patterned templates, they were dipped into an aqueous solution containing Zn^{2+} ions followed by a brief rinsing in deionized water and then dipped into an aqueous solution of S^{2-} ions. This dipping process, which was repeated if necessary, resulted in the formation of ZnS. Interestingly, we found that, after multiple dipping cycles, a high coverage (>98%) of the nanostructured ZnS was formed on the lines of EEEE expressed phage. Optical (Fig. 4B) and AFM (Fig. 4A1 and 4B1) micrographs showed that continuous nanostructured films of ZnS were formed on top of the EEEE-modified phage assembled on the patterned templates. Also, Fig. 4C shows the growth of nanostructured ZnS films on the assembled EEEE-modified phage as a function of the number of dips into the S^{2-} solution. As the number of dipping cycles increased, the average thickness of the nanostructured ZnS increased, reaching up to ~10±2 nm after 50 cycles of dipping.

We confirmed that the ZnS films grown on the linear templates of the EEEE-modified phage were composed of mainly polycrystalline ZnS. Figure S5 of the ESI† shows scanning electron microscopy (SEM) and transmission electron microscopy (TEM) images of typical nanostructured ZnS films grown on the EEEE-modified phage. High resolution TEM and selected area electron diffraction (SAED) revealed the coexistence of amorphous and polycrystalline ZnS domains. Energy dispersive X-ray spectroscopy (EDS) showed that the films were composed of mostly elemental Zn and S. Electrical measurements on the ZnS films revealed a very low conductivity of ~ 10^8 Ω•cm, which was likely due to high density of defects such as dislocations and stacking faults (see Fig. S5 in ESI†).

Why the coverage of ZnS on the assemblies of EEEE-modified M13 phage was higher than that formed on the patterns of immobilized ZBP, in which the same EEEE residues are present is uncertain, but a potential explanation is that the hierarchical arrangement of the peptides in the *pVIII* major coat protein of the phage plays a significant role in enhancing nucleation. This suggests that ion-binding alone is not sufficient to drive ZnS templating with high fidelity and, therefore, reduction of interfacial energy through the collective action of an ensemble of peptides binding to the nascent ZnS crystal surface[18] is also important, as discussed above. Thus the particular arrangement of the EEEE-modified peptides on phage selected to optimize ZnS binding interactions[28] may significantly influence the rate of ZnS nucleation and, consequently, the coverage of ZnS.

Conclusions

We demonstrated that patterned templates of functional peptides and M13 bacteriophage mediate the formation of inorganic materials such as Au and ZnS in mild conditions. Alternating stripes of ODT and TA-PEG-Mal or cysteamine were fabricated on Au surfaces via μ-contact soft lithography followed by the selective immobilization of functional peptides such as GBP and ZBP, as well as whole M13 bacteriophage. These templates were used to mediate the subsequent formation of Au and ZnS nanostructures.

When GBP was immobilized on the patterned templates and reacted in growth solution, Au nanoparticles were successfully formed on the templates. The presence of Ag^+ ions in the growth solution resulted in nearly continuous films of Au nanoparticles with a narrower size distribution. When three different ZBPs were similarly immobilized on the templates and reacted in growth solutions, ZnS nanoparticles were formed on each template but their coverage was significantly less than that obtained during Au nucleation on GBP patterns. In contrast, nanostructured ZnS films exhibiting high coverage were formed on EEEE-modified patterns of M13 bacteriophage when they were subject to multiple cycles of dipping in Zn^{2+} and S^{2-} solutions, even though the terminal group consisted of the same EEEE tetra-glutamate residues were present in the ZBP and genetically expressed on the *pVIII* major coat protein of the M13 bacteriophage. The differences in the behaviour of the GBPs and the ZBPs are in qualitative agreement with expectations based on two distinct mechanisms of nucleation control: enhanced ion binding by GBPs and reduced interfacial energy by ZBPs. However, ion binding must also play a role in ZnS formation on ZBPs and a significant amount of quantitative *in situ* data on rates as a function of supersaturation would be required to prove which mechanism dominates in each case.

Our results demonstrate the technological potential of biomolecule-immobilized templates fabricated via surface patterning techniques for applications that require arbitrary arrangements of nanostructured materials, because they can serve as a powerful guide to assembly of hierarchical nanostructures with multiple material compositions in a spatially-defined fashion.

Experimental section

Synthesis of linker molecules for immobilizing functional peptides

The synthesis of functionalized alkanethioacetate was accomplished using a solid-phase synthesis strategy reported previously.[12] Briefly, 2-trityl chloride resin is loaded with 11-mercaptoundecanoic acid which is subsequently extended via an amide formation with mono-Fmoc-1,4-diaminobutane. The terminal amine is deprotected, acylated with various carboxylic acids, and functionalized with a polyethyleneglycol (PEG)-like linker and handles for further derivatization or reaction with molecules (Quanta BioDesign, Powell, OH, USA). In all cases, the final products were fully deprotonated and cleaved from the solid support by acidolytic cleavage. The functionalized linker molecules as the final products were purified and isolated using preparative-scale, reverse-phase high-performance liquid chromatography (HPLC) and normal-phase column chromatography. The reaction mixtures and purified products were characterized by analytical reverse-phase HPLC and liquid chromatography/electrospray ionization mass spectroscopy (LC/ESI-MS). The syntheses of maleimide-terminated PEG containing thioacetate (TA_PEG-Mal) used in this work were synthesized in a similar manner reported previously.[12]

The synthesis of functional peptides was also accomplished using a solid-phase peptide synthesizer. Gold (Au) binding peptide (GBP) and zinc sulfide (ZnS) binding peptide (ZBP) were discovered via phage display technique.[16] Synthesized GBP has a peptide sequence of *N*-terminus-VSGGSSPDS-GGG-C-*C* terminus. Synthesized ZBP has three different peptide sequences such as *N*-terminus-BISNHAESSRRL-GGG-C-*C*-terminus, *N*-terminus-EEEE-GGG-C-*C*-terminus, and *N*-terminus-EEEE-EEEE-GGG-C-*C*-terminus. In all cases, the final products of GBP and ZBP were purified and isolated using preparatory HPLC and column chromatography. Purified products were also fully characterized by analytical HPLC and LC/ESI-MS.

Preparation of chemically patterned substrates via a μ-contact soft lithography

The approach to fabricating chemical templates for immobilizing functional peptides such as GBP and ZBP and M13 bacteriophage is shown in Fig. 1. Au coated Si substrates were prepared by thermally evaporating ~10 nm of titanium adhesion layer followed by ~150 nm Au on Si (100) wafer. Chemically patterned surfaces with alternating stripes of 1-octadecanethiol (ODT) and linker molecule were produced via μ-contact soft lithography.[32] First, alkyl chain-terminated stripes were deposited by bringing an ODT-coated polydimethylsiloxane (PDMS) elastomer stamp into contact with the freshly prepared Au surface for 10−15 s. Those regions of the Au substrate left bare after the stamping procedure were functionalized with either maleimide or amine moieties by immersing the stamped Au surface in a 200 proof, ~1 mM ethanolic solution of TA-PEG-Mal or cysteamine (HS-$(CH_2)_2$-NH_2) linker overnight. All substrates were thoroughly rinsed with 200-proof fresh ethanol (AAPER Alcohol & Chemical, Shelbyville, KY) and 18.5 MΩ Nanopure™ water (Model Milli-Q RG, Millipore, Billerica, MA, USA) and dried with a stream of ultra-high pure (UHP) N_2 gas.

Characterization of chemically patterned substrates via lateral force microscopy

Lateral force microscopy (LFM) images were collected using CP II atomic force microscope (Veeco Instruments Inc., Santa Barbara, CA) equipped with a silicon nitride cantilever (Sharpened Microlever A, force constant = ca. 0.05 N/m) and a 120 μm close-looped scanner. A typical scan speed of 2−4 Hz was used to acquire a LFM image of 256 X 256 or 512 X 512 pixels. LFM images were analysed by using image processing and analysis software such Nanoscope off-line image analysis (Veeco Instruments Inc., Santa Barbara, CA) and scanning probe image processor (SPIP, Image Metrology A/S).

Immobilization of functional peptides and M13 bacteriophage on chemically patterned substrates

Immobilization of functional peptides on the chemically patterned substrates was accomplished via the following steps. The chemically patterned substrates with alternating stripes of TA-PEG-Mal linker and ODT were immersed in a freshly prepared, ~2 mg/mL solution of functional peptides (such as GBP and ZBP) in a 1X Saline PBS aqueous buffer (pH = 7.4) overnight. Terminal Cysteine (Cys or C) residues of these peptides have a high affinity for covalently binding the maleimide group of TA-PEG-Mal linker via Michael addition reaction. All substrates were rinsed thoroughly with a fresh 1X Saline PBS aqueous buffer and 18.5 MΩ Nanopure™ water and dried with a stream of UHP N_2 gas.

Immobilization of M13 bacteriophage on the chemically patterned substrates was completed via the following procedure.[30] First, terminal EEEE residues were genetically expressed on the *pVIII* major coat protein of the phage. The major coat proteins (~ 50 amino acid long) along the length of the phage with the terminal EEEE residues are displaced at every *N*-terminal group of ~ 2,700 copies of *pVIII* coat protein that is exposed to an outer environment. The chemically patterned substrates with alternating stripes of cysteamine and ODT were immersed in a freshly prepared, ~1 mg/mL solution of phage with the terminal EEEE residues in a 1X Saline PBS aqueous buffer (pH = 7.4) for ~6 hours. All substrates were then rinsed thoroughly with Nanopure™ water and dried with a stream of ultra-high pure (UHP) N_2 gas.

Templated growth of Au and ZnS nanostructures on functional peptides and M13 bacteriophage immobilized chemical templates

Growth of Au on GBP immobilized chemical templates was accomplished through the following procedure. GBP immobilized chemical templates were immersed in ~1 mM aqueous auric acid ($HAuCl_4$) solution for 3−6 hours. In some cases, a small amount of silver acetate ($AgOOCH_3$) was added to the solution as an additive. Typically the relative amount of Au and Ag in the solution ranges from ~99:1 to ~70:30 wt%. Then, the templates were rinsed with 18.5 MΩ Nanopure™ water and then immersed in ~ 1 M aqueous D(+)-glucose solution for 1−6 hours. Finally, the substrates were rinsed thoroughly with Nanopure™ water and dried under gentle UHP N_2 flow.

The growth of ZnS on ZBP and phage immobilized chemical templates was done via similar steps. Following the attachment of ZBP and phage with the terminal EEEE residues on the chemically patterned substrates, the substrates were immersed in a zinc (II) (Zn^{2+}) ion containing aqueous solution (~1 mM of aqueous $ZnCl_2$ solution) for ~10 minutes followed by a brief rinsing in Nanopure™ water and then immersed in a sulfide (S^{2-}) ion containing solution (~1 mM of aqueous Na_2S solution) for ~10 minutes. If necessary, this dipping process was repeated until a desired thickness of ZnS was obtained. Then, the substrates were rinsed with Nanopure™ water dried under gentle UHP N_2 flow.

Characterization of Au and ZnS nanostructures grown on GBP, ZBP, and M13 bacteriophage immobilized chemical templates

Atomic force microscopy (AFM) was used to acquire topography and phase images in tapping mode using a multimode AFM (Nanoscope V controller, Bruker Nano AXS, Santa Barbara, CA) equipped a vertical engagement 160-μm "JV" scanner and a silicon cantilever (FM, Nanoworld, Switzerland, force constant = ca. 2.8 N/m with resonance frequency of 65 kHz) and with a typical scan speed of 0.5−1 Hz. The coverage of Au and ZnS nanostructures was evaluated either by measuring unoccupied areas per given patterned area or counting the number of particles per given area using both Nanoscope image processing program (Bruker Nano AXS, Santa Barbara, CA) and SPIP (Scanning Probe Image Processor, NanoScience Instruments, Inc.). These analyses were performed on at least 5 different samples on ~1X1 μm^2 area.

Transmission electron microscopy (TEM, JEOL FETEM 21000F with 200 kV accelerating voltage) and scanning electron microscopy (SEM, Zeiss Gemini Ultra-55 FESEM) equipped with an Oxford X-ray energy dispersive spectrometer (EDS) for elemental analysis were used to analyse the Au nanostructures on the patterns of GBP, ZnS on ZBP and M13 bacteriophage with terminal EEEE residues. TEM samples were prepared in two different ways. First, Au and ZnS nanoparticles were collected by carefully scraping them off the SAM surface functionalized with GBP or ZBP or modified M13 phage and were put on 200-mesh carbon-coated copper TEM grids. Second, samples were prepared on ~100 nm thick silicon oxide membrane window grids (SPI Supplies, USA) that were treated with a bifunctional linker such as Silane PEG Maleimide (Nanocs Inc., USA) to modify the silicon oxide surface with maleimide functional groups, or Silane PEG Amine (Nanocs Inc., USA) with primary amine groups, respectively. Then, GBP or ZBP or modified M13 were selectively immobilized to induce the formation of Au and ZnS nanoparticles. Also, X-ray photoelectron spectroscopy (XPS, PHI 5400 XPS system) was used to analyse the Au nanostructures on the patterns of GBP, ZnS on ZBP and M13 bacteriophage with terminal EEEE residues.

Conflicts of interest

There are no conflicts to declare.

Acknowledgements

This work was performed at the Molecular Foundry, Lawrence Berkeley National Laboratory under U.S. Department of Energy (DOE) under Contract No. DE-AC0205CH11232. We gratefully acknowledge support from Defence Advanced Research Project Agency (DARPA) program on Tip-Based Nanofabrication (TBN). SWC acknowledges support from the Basic Science Research Program through the National Research Foundation of Korea (NRF), funded by the Ministry of Education, Korea (NRF-2015R1D1A1A01059580). WJC acknowledges support from the Basic Science Research Program through the National Research Foundation of Korea (NRF), funded by the Ministry of Education, Korea (NRF-2017R1A6A1A03015642).

Notes and references

1. B. P. Gray and K. C. Brown, *Chem. Rev.*, 2014, **114**, 1020-1081.
2. S. W. Lee, C. Mao, C. E. Flynn and A. M. Belcher, *Science*, 2002, **296**, 892-895.
3. M. Sarikaya, C. Tamerler, A. K. Jen, K. Schulten and F. Baneyx, *Nat. Mater.*, 2003, **2**, 577-585.
4. S. R. Whaley, D. S. English, E. L. Hu, P. F. Barbara and A. M. Belcher, *Nature*, 2000, **405**, 665-668.
5. M. B. Dickerson, K. H. Sandhage and R. R. Naik, *Chem. Rev.*, 2008, **108**, 4935-4978.
6. C. L. Chen and N. L. Rosi, *Angew. Chem. Int. Ed.*, 2010, **49**, 1924-1942.
7. L. M. Hamm, A. J. Giuffre, N. Han, J. H. Tao, D. B. Wang, J. J. De Yoreo and P. M. Dove, *Porc. Natl. Acad. Sci. U.S.A.*, 2014, **111**, 1304-1309.
8. P. Atanasova, D. Rothenstein, J. J. Schneider, R. C. Hoffmann, S. Dilfer, S. Eiben, C. Wege, H. Jeske and J. Bill, *Adv. Mater.*, 2011, **23**, 4918-4922.
9. D. Rothenstein, S. J. Facey, M. Ploss, P. Hans, M. Melcher, V. Srot, P. A. van Aken, B. Hauer and J. Bill, *Bioinspir. Biomim. Nan.*, 2013, **2**, 173-185.
10. A. S. Schenk, S. Eiben, M. Goll, L. Reith, A. N. Kulak, F. C. Meldrum, H. Jeske, C. Wegeb and S. Ludwigs, *Nanoscale*, 2017, **9**, 6334-6345.
11. N. C. Seeman and A. M. Belcher, *Proc. Natl. Acad. Sci. U.S.A.*, 2002, **99 Suppl 2**, 6451-6455.
12. C. L. Cheung, S. W. Chung, A. Chatterji, T. W. Lin, J. E. Johnson, S. Hok, J. Perkins and J. J. De Yoreo, *J. Am. Chem. Soc.*, 2006, **128**, 10801-10807.
13. S. W. Chung, A. D. Presley, S. Elhadj, S. Hok, S. S. Hah, A. A. Chernov, M. B. Francis, B. E. Eaton, D. L. Feldheim and J. J. Deyoreo, *Scanning*, 2008, **30**, 159-171.
14. J. L. Wilbur, H. A. Biebuyck, J. C. Macdonald and G. M. Whitesides, *Langmuir*, 1995, **11**, 825-831.
15. T. K. Sau and C. J. Murphy, *J. Am. Chem. Soc.*, 2004, **126**, 8648-8649.
16. J. H. Joo, J. F. Hodelin, E. L. Hu and E. D. Haberer, *Mater. Lett.*, 2012, **89**, 347-350.
17. P. J. M. Smeets, K. R. Cho, R. G. E. Kempen, N. A. J. M. Sommerdijk and J. J. De Yoreo, *Nat. Mater.*, 2015, **14**, 394-399.
18. J. J. De Yoreo and P. G. Vekilov, in *Biomineralization*, eds. P. M. Dove, J. J. DeYoreo and S. Weiner, Mineralogical Soc America, Washington, 2003, vol. 54, pp. 57-93.
19. A. J. Giuffre, L. M. Hamm, N. Han, J. J. De Yoreo and P. M. Dove, *Proc. Natl. Acad. Sci. U.S.A.*, 2013, **110**, 9261-9266.
20. Q. Hu, M. H. Nielsen, C. L. Freeman, L. M. Hamm, J. Tao, J. R. I. Lee, T. Y. J. Han, U. Becker, J. H. Harding, P. M. Dove and J. J. De Yoreo, *Faraday Discuss.*, 2012, **159**, 509-523.
21. J. Aizenberg, A. J. Black and G. M. Whitesides, *Nature*, 1999, **398**, 495-498.
22. J. R. I. Lee, T. Y. J. Han, T. M. Willey, D. Wang, R. W. Meulenberg, J. Nilsson, P. M. Dove, L. J. Terminello, T. van Buuren and J. J. De Yoreo, *J. Am. Chem. Soc.*, 2007, **129**, 10370-10381.
23. A. M. Travaille, J. J. J. M. Donners, J. W. Gerritsen, N. A. J. M. Sommerdijk, R. J. M. Nolte and H. van Kempen, *Adv. Mater.*, 2002, **14**, 492-+.
24. D. M. Duffy and J. H. Harding, *Langmuir*, 2004, **20**, 7630-7636.
25. C. L. Freeman, Q. Hu, M. H. Nielsen, J. Tao, J. J. De Yoreo and J. H. Harding, *J. Phys. Chem. C*, 2013, **117**, 5154-5163.
26. C. J. Munro, Z. E. Hughes, T. R. Walsh and M. R. Knecht, *J. Phys. Chem. C*, 2016, **120**, 18917-18924.
27. T. Sakai and P. Alexandridis, *J. Phys. Chem. B.*, 2005, **109**, 7766-7777.
28. C. Mao, C. E. Flynn, A. Hayhurst, R. Sweeney, J. Qi, G. Georgiou, B. Iverson and A. M. Belcher, *Proc. Natl. Acad. Sci. U.S.A.*, 2003, **100**, 6946-6951.

29. K. T. Nam, D. W. Kim, P. J. Yoo, C. Y. Chiang, N. Meethong, P. T. Hammond, Y. M. Chiang and A. M. Belcher, *Science*, 2006, **312**, 885-888.
30. S. Y. Yoo, W. J. Chung, T. H. Kim, M. Le and S.-W. Lee, *Soft Matter.*, 2011, **7**, 363-368.
31. D. A. Marvin, L. C. Welsh, M. F. Symmons, W. R. Scott and S. K. Straus, *J. Mol. Biol.*, 2006, **355**, 294-309.
32. J. L. Wilbur, A. Kumar, E. Kim and G. M. Whitesides, *Adv. Mater.*, 1994, **6**, 600-604.

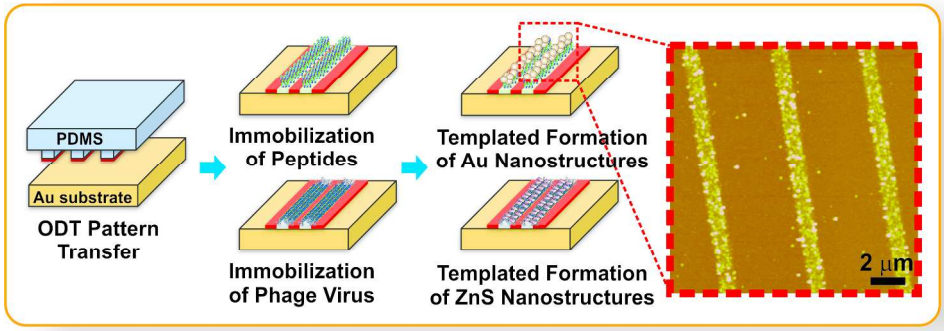

Directed nucleation of Au and ZnS nanopatterns is performed on templates comprised of functional peptides and M13 bacteriophage.

274x117mm (300 x 300 DPI)